

COPPER ELECTROLESS PLATING IN PRESENCE OF COBALT IONS USING HYPOPHOSPHITE AS REDUCTANT

<http://dx.medra.org/10.19228/j.cpm.2016.35.03>

J. I. Martins^{1,2,*}, M. C. Nunes¹ and P. B. Tavares³

¹ Universidade do Porto, Faculdade de Engenharia, Departamento de Engenharia Química, Rua Roberto Frias, 4200-465 Porto, Portugal.

² Lab2PT, Instituto de Ciências Sociais, Universidade do Minho, Campus do Gualtar, 4710-057 Braga, Portugal, mcnunes@fe.up.pt

³ Centro de Química - Vila Real, ECVA, Universidade de Trás-os-Montes e Alto Douro, 5001-801 Vila Real, Portugal, ptavares@utad.pt

*A quem a correspondência deve ser dirigida, jipm@fe.up.pt

ABSTRACT

The electroless copper plating using sodium hypophosphite as the reductant and sodium citrate as the chelating agent was studied by gravimetric and electrochemical measurements. The effects of temperature, pH, boric acid, citrate, hypophosphite, and cobalt catalyst concentration were evaluated.

The kinetics of the electroless copper deposition was interpreted on the basis of the dehydrogenation of the reductant, mixed potential theory, and in the ionic speciation of the bath.

Scanning electron microscopy, X-ray microanalysis by energy dispersive spectroscopy and X-ray diffraction applied on surfaces show that the deposits are composed by binary (Cu-Co) and ternary alloys (Cu-Co-P), and that their morphology and crystallinity depends on cobalt and phosphorus content.

Keywords: *Electroless, Copper Plating, Sodium Hypophosphite, Ionic Speciation, Copper-Cobalt Alloys*

DEPOSIÇÃO DE COBRE NÃO ELECTROLÍTICO NA PRESENÇA DE IÕES DE COBALTO UTILIZANDO O HIPOFOSFITO COMO REDUTOR

RESUMO

O revestimento de cobre não electrolítico usando hipofosfito de sódio como redutor e o citrato de sódio como agente complexante foi estudado através de medições gravimétricas e electroquímicas. Avaliaram-se os efeitos da temperatura, pH, ácido bórico, citrato, hipofosfito e concentração do catalisador de cobalto.

A cinética de deposição de cobre não electrolítico foi interpretada na base da desidrogenação do redutor, teoria do potencial misto e na especiação iónica do banho.

A microscopia electrónica de varrimento, microanálise de raios X por espectroscopia de dispersão de energia e a difracção de raios-X aplicada nas superfícies mostram que os depósitos são constituídos por ligas binárias (Cu-Co) e ternárias (Cu-Co-P), e que a sua morfologia e cristalinidade depende do teor de cobalto e fósforo.

Palavras-chave: *Revestimento não Electrolítico, Deposição de Cobre, Hipofosfito de Sódio, Especiação Iónica, Ligas de Cobre-cobalto*

1. INTRODUCTION

Copper electroless plating has been an important field in industry to produce articles for decorative and functional purposes, such as dielectrics [1], printed circuit boards [2], insulating substrates [3, 4] and patterns of complex geometry [5]. Autocatalytic metal plating on polymer substrates is particularly interesting on flexible and transparent device applications. The physicochemical properties of autocatalytic deposits of copper and nickel are closely dependent on the composition of the baths and respective operating conditions [6, 7]. Hence, the interest of researchers about the kinetic phenomena involved at the metal/solution interface in electroless plating systems [8-10].

Common electroless copper baths use i) formaldehyde [11], as the reducing (ii) sodium potassium tartrate (called as "Rochelle salt"), sodium malate, sodium citrate, triethanolamine (TEA), ethylenediamine (En), or ethylenediamine tetraacetic acid (EDTA), as complexing agents, (iii) boric acid, or succinic acid as a buffer, (iv) sulfur-containing compounds (sulfite, thiosulfates, sulfates), nitrogen-containing compounds (tetracyanoethylene, cyanides, pyridines, 2,2'-pyridil), or sulfur- and nitrogen-containing compounds (cysteines, cystines, diethyldithiocarbamates, thiosemicarbazide, thiourea) as stabilizers, and (v) cyanide or propionitrile, as additives for accelerating the reaction.

Formaldehyde baths produces high quality copper with excellent electrical and mechanical properties at low-cost and widely available. However, formaldehyde has been listed recently as a hazardous material. Therefore, many researchers have sought other electroless copper solutions using nonformaldehyde reducing agents such as sodium hypophosphite [12, 13], dimethylamine borane (DMBA) [14, 15], hydrazine [16], glyoxylic acid [17], Co(II) [18], Fe(II) [19], sodium bisulphite and sodium thiosulfate [20]. Among them, the coating process based on hypophosphite has been the subject of enough research because of its safety, low price, good bath stability, and relatively easy to control plating conditions. However, the hypophosphite-based electroless copper plating process is difficult since copper does not catalyze the oxidation of hypophosphite. One approach to perform the oxidation of the reducing agent is to add cobalt [21] or nickel [22] ions to the bath, since cobalt and nickel catalyze the oxidation of hypophosphite.

The use of complexing agents in the baths aims to control the effective availability of copper ion in the desired cathodic reaction. The stability of the bath, grain size and the composition of the binary Cu-Co or ternary Cu-Co-P alloys depend on the ionic speciation of the solution, i.e., the resulting complexes of copper ion and the ligand. The coordination numbers of copper complexes are six or four, and their geometric forms are octahedral and tetrahedral or square planar, respectively. However, on the structural perspective, it is difficult to distinguish between these three structures [23, 24].

A chemical displacement process requires that the solid side of the interface is not equipotential. Thus, there may be the occurrence of a redox couple associated with the oxidation of a reductant (R) on the anodic areas and the reduction of metallic ions (M^{n+}) on the cathodic areas.



After soaking the solid surface in the electroless bath closes the electrochemical circuit, and the phenomena of polarization in the

cathodic and anodic areas impose opposite signal overpotentials (η). In the absence of an ohmic drop in steady state, the surface is practically equipotential, i.e., works under the mixed potential (E_{MP}).

$$\text{Anodic overpotential: } \eta_R = E_{MP} - E_R \quad (3)$$

$$\text{Cathodic overpotential: } \eta_M = E_{MP} - E_M \quad (4)$$

According to the Wagner-Traud postulate [25], the plating rate i_p is given by,

$$i_p = \sum_{j=1}^n i_{Rj} = \left| \sum_{j=1}^n i_{Mj} \right| \quad (5)$$

where i_{Rj} and i_{Mj} are the anodic and cathodic partial currents of the reactions in plating system.

The cathodic and anodic phenomena, in the absence of convection, will be interpreted as exclusively being controlled by diffusion or activation.

In diffusional control the current is independent of potential and takes the form [26]:

$$i = \frac{nFAD(C^b - C^s)}{\delta} \quad (6)$$

where D is the diffusion coefficient, δ the diffusion layer thickness, A the area of the sample, n the number of electrons, F the Faraday constant, and C^b and C^s the concentrations of the electroactive species, respectively, in the bulk solution and on the surface.

If the concentration of the electroactive species on the metal interface is null, the expression (6) takes the form of so-called limiting current:

$$i_L = \frac{nFADC^b}{\delta} \quad (7)$$

When the electrochemical phenomena are controlled by activation under strong field, the current is related exponentially to the overpotential by Tafel equation:

$$i = i^0 \exp\left(\frac{\eta}{\beta}\right) \quad (8)$$

where i^0 and β are the Tafel parameters.

The mixed potential on the solid surface therefore depends on the type of control established in the system. Thus, in a system where cathodic and anodic reactions are under diffusion and activation control, respectively, the surface potential is:

$$E_{MP} = E_R^0 + \frac{RT}{nF} \ln C_R^b + \beta_R \ln \frac{nFAD_M C_M^b}{\delta} - \beta_R \ln i_R^0 \quad (9)$$

In the case in which the cathodic reaction is controlled by activation and anodic reaction by diffusion, the surface potential is then:

$$E_{MP} = E_M^0 + \frac{RT}{nF} \ln C_M^b + \beta_M \ln \frac{nFAD_R C_R^b}{\delta} + \beta_M \ln i_M^0 \quad (10)$$

The goal of this work is to study the kinetics, morphology and crystallinity of copper-cobalt alloys from electroless process with hypophosphite as reductant.

2. EXPERIMENTAL

2.1. Chemicals and solutions

The standard bath solution consists of 0.024 M copper sulphate ($CuSO_4 \cdot 5H_2O$), 0.27 M sodium hypophosphite ($NaH_2PO_2 \cdot H_2O$), 0.052 M

sodium citrate ($\text{Na}_3\text{C}_6\text{H}_5\text{O}_7 \cdot 2\text{H}_2\text{O}$), 0.50 M boric acid (H_3BO_3), and 0.004 M cobalt sulphate ($\text{CoSO}_4 \cdot 6\text{H}_2\text{O}$), pH was adjusted to 10.0 with sodium hydroxide or sulphuric acid, and temperature 65 °C. All chemicals were reagent grade, and deionized water was used to prepare the solutions.

2.2. Plating procedure

A volume of 80 mL plating bath was placed in a four-neck Pyrex Quickfit vessel 120 mL capacity with a heating jacket. The temperature was controlled with accuracy ± 0.5 °C, and a spiral condenser was placed to maintain the atmospheric pressure and eliminate the water losses. The volume of the bath was considered to be enough to guarantee a system in steady state during 30 minutes of deposition. The alkalinity of the solutions was evaluated with accuracy ± 0.02 pH units using a Cryson 2002 apparatus.

Aluminium (99 %) sheets ($1.5 \times 1.0 \times 0.3 \text{ cm}^3$) placed in a glass support were used as a substrate for deposits of Cu-Co alloys. The samples prior to be suspended into the plating solution were pre-treated according to the following operative sequence: clean-up with acetone; alkaline degreasing ($30 \text{ g L}^{-1} \text{ Na}_2\text{CO}_3$, $8 \text{ g L}^{-1} \text{ Na}_2\text{SiO}_3$, $T = 80$ °C, $t = 2-4$ min); acid pickling (HNO_3 50 % v/v, $T = 40$ °C, $t = 2$ min); and washing with deionized water.

Metal deposition rate was determined by weight change of initial aluminium boards to the end plating process, after appropriate rinsing, immersion in ketone, and drying. The aluminum content in the end of the tests was determined by atomic absorption spectroscopy (AAS) using a Perkin Elmer Model 5100PC for possible correction of these measures.

2.3. Electrochemical procedures

The electrochemical experiments were performed in one-compartment cell with three electrodes connected to Autolab model PGSTAT20 potentiost/galvanostat with pilot integration controlled by GPES 4.4 software. The working electrode rod (1 cm diameter) was aluminium, copper or cobalt 99 %. The electrodes were mechanically polished with abrasive paper (1200-grade) and rinsed with water before each electrochemical experiment. Platinum was used as auxiliary electrode, and potentials were measured versus an Ag/AgCl (1.0 M KCl) or SCE reference electrode.

2.4. Microscopy, spectroscopy and X-ray diffraction analysis

The scanning electron microscopy (SEM) images and the analysis by energy dispersive X-ray spectroscopy (EDS) were made with a FEI Quanta 400FEG, fitted with an EDAX Genesis X4M micro analysis probe, in CEMUP.

The X-ray diffraction patterns were acquired on ABS samples with copper deposits obtained at different $[\text{Co}^{2+}]_{\text{total}} / [(\text{Co}^{2+} + \text{Cu}^{2+})]_{\text{total}}$ mole ratio in the solutions, and also at different temperatures for the standard bath composition.

ABS [polybutadiene block grafted by styrene acrylonitrile copolymer] samples were subjected to a pretreatment before the metallization process, according to the following procedure: 1) degreasing in alkaline solution - $20 \text{ g L}^{-1} \text{ Na}_2\text{CO}_3$ + 10 g L^{-1} sodium gluconate + $30 \text{ g L}^{-1} \text{ Na}_3\text{PO}_4$ + 1.5 g L^{-1} sodium dodecyl (ester) sulfate, at 65 °C with stirring for 10 min; 2) washing in water at 65 °C with stirring for 5 min; 3) etching with chromic solution to provide hydrophilic and micro-roughened surface - $375-425 \text{ g L}^{-1} \text{ H}_2\text{CrO}_4$ + $180-220 \text{ mL L}^{-1} \text{ H}_2\text{SO}_4$ (98 %), at 65-70 °C with stirring for 12-15 min; 4) washing with water at 25 °C with stirring for 6 min; 5) conversion of Cr (VI) to Cr (III) in $30 \text{ g L}^{-1} \text{ NaHSO}_3$ solution, at 25°C with stirring

for 2-3 min; 6) washing in water at 25° C with stirring for 4 min; 7) pre-activation in HCl (30 %) solution with stirring at 25 °C for 4 min; 8) sensitization in $10 \text{ g L}^{-1} \text{ SnCl}_2$ + $60 \text{ mL L}^{-1} \text{ HCl}$ (37 %), at 30-32 °C with moderate stirring for 5 min; 9) washing with water at 25 °C with moderate stirring for 1-2 min; 10) activation to produce catalytic sites that will enable chemical deposition of nickel or copper in $0.5 \text{ g L}^{-1} \text{ PdCl}_2$ + $20 \text{ mL L}^{-1} \text{ HCl}$ (37 %) at 40 °C for 5 min; 11) washing with water at 25 °C with moderate agitation for 4 min; 12) post activation or acceleration in a $50 \text{ g L}^{-1} \text{ H}_2\text{SO}_4$ (98 %) at 25 °C with moderate stirring for 2-4 min; 13) washing in water at 25 °C with moderate stirring for 4 min.

The X-ray diffraction (XRD) spectra was carried out in a PANalytical X'Pert Pro MPD equipped with a X'Celerator detector and secondary monochromator (Cu $K\alpha = 0.154 \text{ nm}$, 40 kV, 30 mA; data recorded with 0.017 step size, 100 s/step). The species identification was performed through the HighScore Plus software with the ICDD database. Rietveld refinement with PowderCell software (CCP14, Federal Institute for Materials Research and Testing) was used to calculate lattice parameters and crystallite size from the XRD diffraction patterns.

The content of copper, cobalt and phosphorus inside the deposit was determined directly on the coating by SEM/EDS, and also by AA after dissolving the same in nitric acid solution.

3. CHEMICAL MODEL TO COPPER PLATING SYSTEM

The chemical model [22] proposed for the determination of the composition of the copper plating solutions, twenty five species, includes nineteen correlations, equations (11) to (29) listed in Table 1, and the following material and charge balances:

$$\text{Citrate: } C_1 = X_1 + X_5 + X_6 + X_7 + X_{12} + X_{13} + X_{14} + X_{15} \quad (30)$$

$$\text{Boric acid: } C_2 = X_8 + X_9 + X_{10} + X_{11} \quad (31)$$

$$\text{Hypophosphite: } C_3 = X_{24} + X_{25} \quad (32)$$

$$\text{Copper: } C_4 = X_3 + X_{12} + X_{14} + X_{20} + X_{21} + X_{22} + X_{23} \quad (33)$$

$$\text{Cobalt: } C_5 = X_4 + X_{13} + X_{15} + X_{17} + X_{18} + X_{19} \quad (34)$$

$$\text{Charge balance: } 3C_1 + C_3 + X_2 + 2X_3 + 2X_4 + X_{17} + X_{20} = 3X_1 + 2X_5 + X_6 + 3X_8 + 2X_9 + X_{10} + X_{14} + X_{15} + X_{16} + X_{19} + 2X_{23} + X_{22} + 2C_4 + 2C_5 \quad (35)$$

When adjusting the pH with NaOH, the concentration of sodium ion is taken into account in equation (35).

The activity coefficients of the ionic species necessary for to know the factors G_i , Table 1, were calculated from the modified Debye-Hückel equation utilizing the modifications proposed by Robinson and Guggenheim and Bates [27]:

$$-\frac{\log f_i}{z_i^2} = \left[\frac{0.511\sqrt{I}}{1+1.5\sqrt{I}} - 0.2I \right] \quad (36)$$

where z_i is the charge of the ion, and I the ionic strength calculated by the following equation:

$$I = \sum_{j=1}^n X_j z_j^2 \quad (37)$$

Table 1 - Chemical equilibrium in copper plating solutions.

Reaction	Notation	Equilibrium Constant
$\text{HCit}^{2-} = \text{Cit}^{3-} + \text{H}^+$ equation (11)	$X_1 = \text{Cit}^{3-}; X_2 = \text{H}^+; X_5 = \text{HCit}^{2-}$	$K_1 = G_1 X_2 X_5 / X_1$ $\text{p}K_1 = 6.40$ [27]
$\text{H}_2\text{Cit}^- = \text{HCit}^{2-} + \text{H}^+$ equation (12)	$X_6 = \text{H}_2\text{Cit}^-$	$K_2 = G_2 X_5 X_6 / X_1$ $\text{p}K_2 = 4.76$ [27]
$\text{H}_3\text{Cit} = \text{H}_2\text{Cit}^- + \text{H}^+$ equation (13)	$X_7 = \text{H}_3\text{Cit}$	$K_3 = G_3 X_5 X_7 / X_1$ $\text{p}K_3 = 3.13$ [27]
$\text{H}_2\text{PO}_4^- = \text{H}_2\text{PO}_4^- + \text{H}^+$ equation (14)	$X_{24} = \text{H}_2\text{PO}_4^-; X_{25} = \text{H}_3\text{PO}_4$	$K_4 = G_4 X_{24} X_{25} / X_{25}$ $\text{p}K_4 = 1.10$ [27]
$\text{HBO}_3^{2-} = \text{BO}_3^{3-} + \text{H}^+$ equation (15)	$X_8 = \text{BO}_3^{3-}; X_9 = \text{HBO}_3^{2-}$	$K_5 = G_5 X_8 X_9 / X_9$ $\text{p}K_5 = 13.80$ [27]
$\text{H}_2\text{BO}_3^- = \text{HBO}_3^{2-} + \text{H}^+$ equation (16)	$X_{10} = \text{H}_2\text{BO}_3^-$	$K_6 = G_6 X_9 X_{10} / X_{10}$ $\text{p}K_6 = 12.74$ [27]
$\text{H}_3\text{BO}_3 = \text{H}_2\text{BO}_3^- + \text{H}^+$ equation (17)	$X_{11} = \text{H}_3\text{BO}_3$	$K_7 = G_7 X_{10} X_{11} / X_{11}$ $\text{p}K_7 = 9.24$ [27]
$\text{Cu}^{2+} + \text{HCit}^{2-} = \text{CuHCit}$ equation (18)	$X_3 = \text{Cu}^{2+}; X_{12} = \text{CuHCit}$	$K_8 = G_8 X_{12} / X_3 X_5$ $\log K_8 = 9.80$ [28]
$\text{Cu}^{2+} + \text{Cit}^{3-} = \text{CuCit}^-$ equation (19)	$X_{14} = \text{CuCit}^-$	$K_9 = G_9 X_{14} / X_3 X_1$ $\log K_9 = 5.90$ [28]
$\text{Co}^{2+} + \text{HCit}^{2-} = \text{CoHCit}$ equation (20)	$X_6 = \text{Co}^{2+}; X_{13} = \text{CoHCit}$	$K_{10} = G_{10} X_{13} / X_6 X_5$ $\log K_{10} = 10.44$ [29]
$\text{Co}^{2+} + \text{Cit}^{3-} = \text{CoCit}^-$ equation (21)	$X_{15} = \text{CoCit}^-$	$K_{11} = G_{11} X_{15} / X_6 X_1$ $\log K_{11} = 6.19$ [29]
$\text{H}_2\text{O} = \text{OH}^- + \text{H}^+$ equation (22)	$X_{16} = \text{OH}^-$	$K_{12} = G_{12} X_{16}$ $\text{p}K_{12} = 14.00$ [27]
$\text{Cu}^{2+} + \text{OH}^- = \text{CuOH}^+$ equation (23)	$X_3 = \text{Cu}^{2+}; X_{20} = \text{CuOH}^+$	$K_{13} = G_{13} X_{20} / X_3 X_{16}$ $\log K_{13} = 7.00$ [27]
$\text{CuOH}^+ + \text{OH}^- = \text{Cu(OH)}_2$ equation (24)	$X_{21} = \text{Cu(OH)}_2$	$K_{14} = G_{14} X_{21} / X_{20} X_{16}$ $\log K_{14} = 6.68$ [27]
$\text{Cu(OH)}_2 + \text{OH}^- = \text{Cu(OH)}_3^-$ equation (25)	$X_{22} = \text{Cu(OH)}_3^-$	$K_{15} = G_{15} X_{22} / X_{21} X_{16}$ $\log K_{15} = 3.32$ [27]
$\text{Cu(OH)}_3^- + \text{OH}^- = \text{Cu(OH)}_4^{2-}$ equation (26)	$X_{23} = \text{Cu(OH)}_4^{2-}$	$K_{16} = G_{16} X_{23} / X_{22} X_{16}$ $\log K_{16} = 1.50$ [27]
$\text{Co}^{2+} + \text{OH}^- = \text{CoOH}^+$ equation (27)	$X_6 = \text{Co}^{2+}; X_{17} = \text{CoOH}^+$	$K_{17} = G_{17} X_{17} / X_6 X_{16}$ $\log K_{17} = 4.30$ [30]
$\text{CoOH}^+ + \text{OH}^- = \text{Co(OH)}_2$ equation (28)	$X_{18} = \text{Co(OH)}_2$	$K_{18} = G_{18} X_{18} / X_{17} X_{16}$ $\log K_{18} = 4.10$ [30]
$\text{Co(OH)}_2 + \text{OH}^- = \text{Co(OH)}_3^-$ equation (29)	$X_{19} = \text{Co(OH)}_3^-$	$K_{19} = G_{19} X_{19} / X_{18} X_{16}$ $\log K_{19} = 1.30$ [30]

Symbols: X_i = molar fraction of species i ; G_i = factor relating the activity coefficient of the ionic species.

The numerical solution of the equations proposed for the chemical model has been obtained by the Newton-Raphson method [31]. In this model the cobalt and copper are distributed among ionic free form, citrate complexes and hydroxide complexes. Assuming that at the solution/metal interface the cathodic reaction related to metal deposition is a function of the respective positive ionic species in the bath, $[\text{Cu}^{2+}]$, $[\text{CuOH}^+]$, $[\text{Co}^{2+}]$ and $[\text{CoOH}^+]$, we will consider the sum of all these concentrations to interpret the kinetics data.

$$\Sigma_{\text{Cu}} = [\text{Cu}^{2+}] + [\text{CuOH}^+] = X_3 + X_{20} \quad (38)$$

$$\Sigma_{\text{Co}} = [\text{Co}^{2+}] + [\text{CoOH}^+] = X_6 + X_{17} \quad (39)$$

4. RESULTS AND DISCUSSION

4.1. Morphology and crystallinity

The morphology varies significantly with operating conditions, particularly with the $[\text{Co}^{2+}]_{\text{total}} / [(\text{Co}^{2+} + \text{Cu}^{2+})_{\text{total}}]$ mole ratio in the solutions, i.e., the metallic ratio of catalyst (MRC). Fig. 1(a) and 1(b) for MRC = 0.111 (Co1) shows a uniform cubic crystalline structure, as well as for MRC equal to 0.238 (Co2) with a grain size between 0.4 μm and 1 μm . Increasing MRC to 0.500 (Co3) and 0.750 (Co4) the structure changes completely and appears a uniform globular structure (Fig. 1(c)), such as a cauliflower-like of particles with an average size of 10-30 nm (Fig. 1(d) and 1(e)) to form larger clusters

of about 0.7-1.0 μm , Fig. 1(f)), which seems a loss in the crystallinity. Samples Co1, Co2, Co3 and Co4 showed phosphorus weight percentage, respectively, 0.32, 0.43, 1.37 and 2.23 % and the cobalt content 4.42, 5.93, 12.11 and 17.66 %. The deposits with the highest phosphorus (Fig.1(d) and 1(e)) content display some holes related to hydrogen evolution.

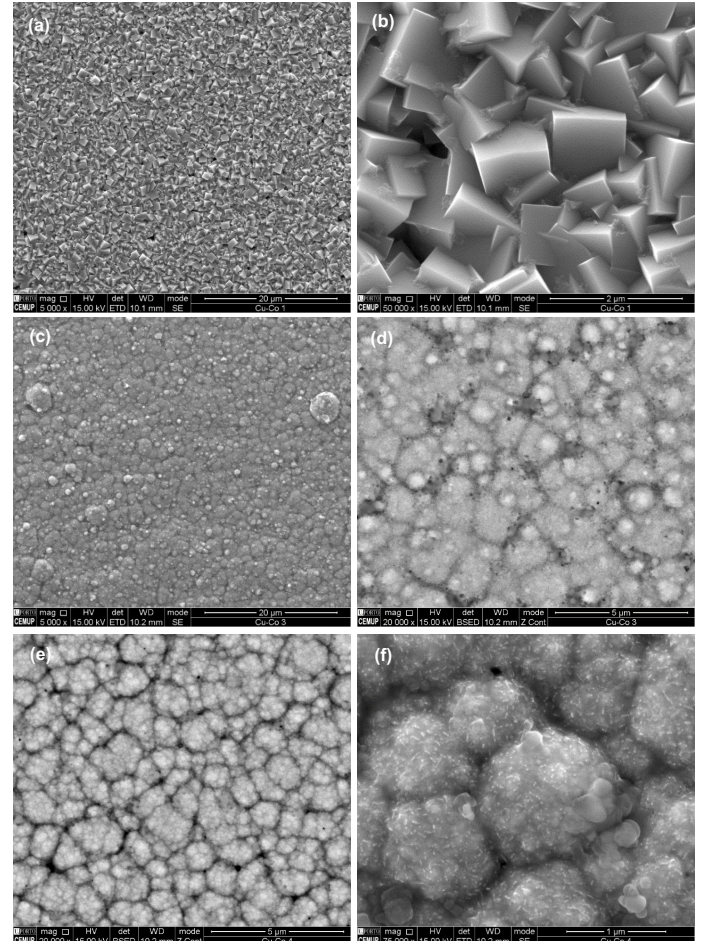


Fig. 1 – SEM micrographs of copper deposits from standard solution with the following alterations: a), b) $[\text{CoSO}_4] = 0.005$ M and $[\text{CuSO}_4] = 0.040$ M, MRC = 0.111; c), d) $[\text{CoSO}_4] = 0.020$ M and $[\text{CuSO}_4] = 0.020$ M, MRC = 0.500; e), f) $[\text{CoSO}_4] = 0.030$ M and $[\text{CuSO}_4] = 0.010$ M, MRC = 0.750.

The XRD patterns of the copper films obtained for different MRC in the bath, Fig. 2, show peaks at $2\theta = 29.8^\circ$ (110), 36.6° (111), 42.3° (200), 61.4° (220), and 73.5° (311), which according to the standard powder diffraction card of JCPDS [32] have been attributed to cuprous oxide (lattice parameter $a = 4.288 \pm 0.001 \text{ \AA}$), and at $2\theta = 43.5^\circ$ (111), 50.6° (200), 74.2° (220), 90.0° (311) and 95.3° (222) attributed to copper (lattice parameter $a = 3.621 \pm 0.001 \text{ \AA}$). The characteristic reflections of the hexagonal cobalt structure could not be found. The magnification of the copper peak (111), Fig. 3, presents a deviation of its position from the Co1 sample to the Co4 sample with a slight increase in the lattice parameter (3.620 to 3.622 \AA). The crystallite sizes, determined by the Williamson-Hall plot, are in the range of 25 ± 5 nm for samples Co1 and Co2, 14 ± 3 nm for sample Co3 and 10 ± 2 nm for sample Co4. According to constitutional phase diagram [33] copper-cobalt alloys constitute mixtures of virtually pure components, but the mutual solubility of the components in solid state is only 1 % w/w. We consider that the cobalt substitutes the copper in the face-centered cubic lattice, thus pointing substitutional solid solutions, as has been already claimed by Povetkin and Devyatkova [34]. The broad peak at around 20 deg is

related to ABS substratum [35]. The difference in the intensity of the peaks is related to the thickness of the copper plating. The observation of the section of the sample Co3 cracked after being immersed in liquid nitrogen, shows a thickness of the order of 3 microns, Fig. 4. This finding confirms the intensity of the peaks observed in samples Co1 and Co2 to $2\theta \cong 20^\circ$ given the EDS depth of field. The detected cuprous oxide particularly on samples Co1 and Co2 comes from their surface oxidation [36] occurred in the time interval that has elapsed between their acquisition and analysis by X-ray diffraction. The X-ray diffraction results show that the Cu-Co-P alloys retain their crystallinity for phosphorus until at least 2% (MRC = 0.75). In the case of Cu-Ni-P alloys for MRC = 0.75 the phosphorus content is about 3 times higher, and these alloys become amorphous for phosphorus content higher than 8.7 % [22].

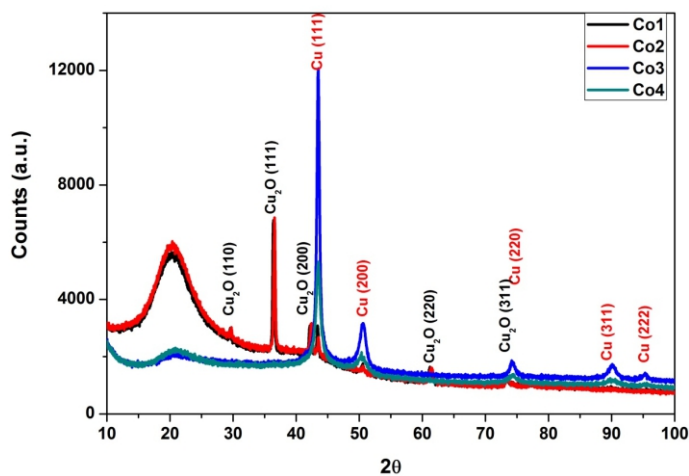


Fig. 2 – XRD patterns of the Cu-Co-P alloys for different ratios between $[CoSO_4]$ and $[(CuSO_4) + [CoSO_4]]$, MRC: a) Co1, MRC = 0.111; b) Co2, MRC = 0.238; c) Co3, MRC = 0.500; Co4, MRC = 0.750.

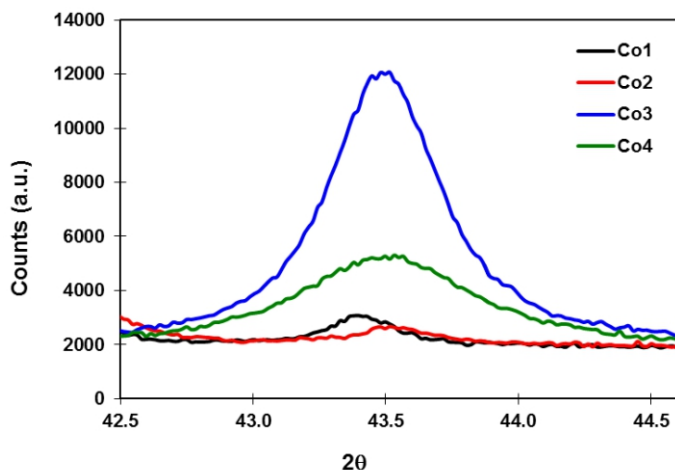


Fig. 3 – Magnification of the [111] copper peak showing the deviation of the peak position in sample Co1 to higher d space value (lower 2θ), possible due to the formation of a solid solution with cobalt.

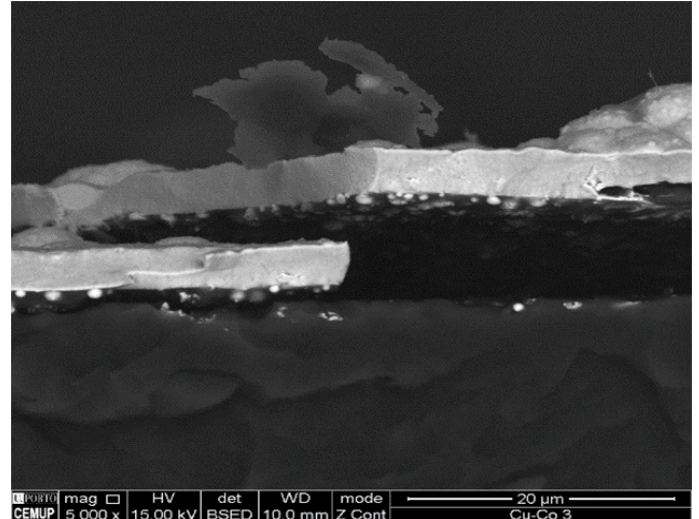


Fig. 4 – SEM micrograph of the cross section of copper film deposited in the ABS for the sample Co3.

4.2. Effect of electroless plating time

The thermodynamic and kinetic feasibility of the electroless process requires the adsorption of hypophosphite on the substrate surface and the breaking of P-H bond, in order to promote its oxidation. The materials able to do this interaction are the so-called catalytic materials, such as nickel, cobalt, gold, and palladium [37]. In the case of aluminum substrate, the cobalt deposition is initiated by galvanic displacement giving rise to the catalytic surface on which, thereafter, the Cu-Co electroless deposit develops. It is obvious that in this early stage of the process there is also a chemical shift of copper.

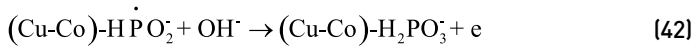
The tests with the standard composition of the bath shows that the thickness of the deposits increases linearly with time over 60 minutes. This means that the solution composition is not significantly affected during this time interval, i.e., there is no interference of composition on the phenomena of charge transfer at the solution-metal interface for anodic and cathodic areas. The average cobalt content in deposits is around 4.5 % and the phosphorus 0.2-0.3 % for time interval between 20 and 60 minutes. Therefore, all the trials have been performed during 30 minutes.

4.3. Effect of cobalt catalyst

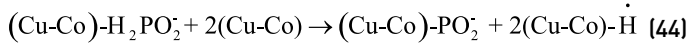
Figure 5 shows the effect of formal concentration of catalyst on the deposition rate and coating composition. There is an increase in overall rate with increasing cobalt content in deposit while the phosphorus remains practically constant. The Σ_{Co} profile increases with the catalyst concentration which justifies the increase in percentage of cobalt in the deposit, and therefore of the catalytic centers responsible for the oxidation of hypophosphite. The dependence of the reaction rate with the proportion of cobalt is less pronounced from 0.003 mol L^{-1} , which is associated with the alloy composition. It is concluded that the reaction is controlled electrochemically. In terms of mechanism and designating the active centers by $[Cu-Co]$, the controlling step of hypophosphite oxidation passes by dehydrogenation on the surface with the formation of a radical [9, 38],



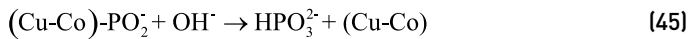
converted immediately into phosphite according to the reaction:



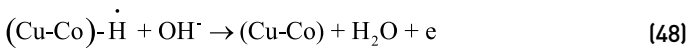
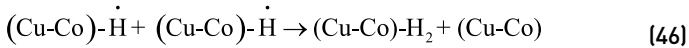
In line with Gutzeit [39] the hypophosphite dehydrogenation passes through the formation of metaphosphite anion,



followed by the formation of phosphite according to:



The atomic hydrogen may be recombined in molecular hydrogen or be oxidized to water.



The cathodic reaction will be:



Table 2 - Influence of pH on deposition rate, ionic speciation of positive copper ions, and alloy composition, for standard bath composition.

Variable	pH				
	9.5	10.0	10.5	11.0	11.5
$v / \text{mg cm}^{-2} \text{h}^{-1}$	4.1	5.4	6.13	7.3	7.6
$\Sigma_{\text{Cu}} / \text{mol L}^{-1}$	1.6×10^{-11}	3.3×10^{-11}	6.0×10^{-11}	1.2×10^{-10}	2.4×10^{-10}
Co / %	5.5	4.7	4.3	4.1	3.8
P / %	0.6	0.5	0.4	0.3	0.2

4.5. Effect of hypophosphite

Figure 6 shows a linear dependence between the concentration of the reductant and the deposition rate. Nevertheless, for higher reducing agent concentrations of 0.6 M the global reaction rate tends to a plateau indicative of a diffusional control for cathodic reaction: $v = 8.3 \text{ mg cm}^{-2} \text{ h}^{-1}$; $\Sigma_{\text{Cu}} = 2.1 \times 10^{-11} \text{ M}$; $\Sigma_{\text{Co}} = 3.1 \times 10^{-14} \text{ M}$; and Cu-4.60Co-0.30P composition alloy. Considering the Faraday equation and alloy composition, the limiting current density for copper deposition is $j_L(\text{Cu}) = 6.7 \text{ mA cm}^{-2}$. The surplus negative charge in the substrate will be consumed in the hydrogen evolution.



The voltammograms obtained from cyclic voltammetry performed on cobalt electrode show that the oxidation of hypophosphite for the pH between 10.0 and 10.5 is in the range of -0.65 to -0.75 V vs. Ag/AgCl, which agree well with the results of Ohno et al [37].

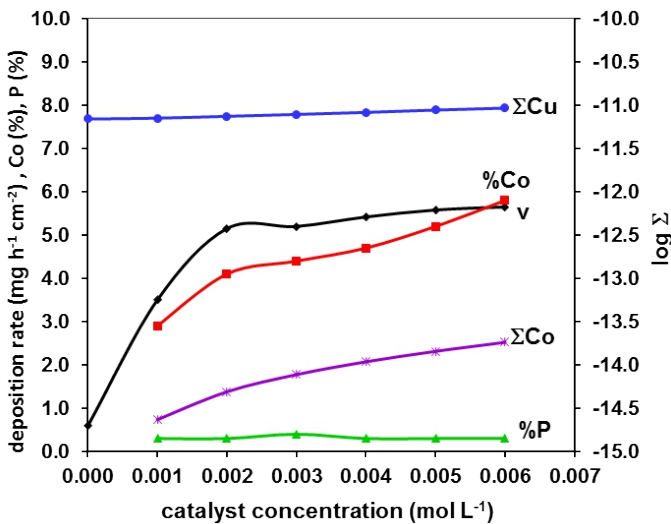


Fig. 5 - Influence of catalyst concentration on deposition rate, ionic speciation of copper and cobalt positive ions, and alloy composition, for standard bath composition.

4.4. Effect of pH

Table 2 shows that the reaction rate increases with pH, an effect of concentration on the step of hypophosphite oxidation, equations (42) or (45). The alkalinity decreases the concentration of solvated species Cu^{2+} and increase the $\text{Cu}(\text{OH})^+$ concentration, an effect of ionic distribution in the bath composition. However, as the Σ_{Cu} concentration of the reaction rate increases with the pH range despite the little reduction in cobalt content in the alloy, it must be admitted that the deposition rate depends on all positive ions in solution. Thus, removal of the hydroxyl ion in the metallic complexes takes place simultaneously with the step of charge transfer.

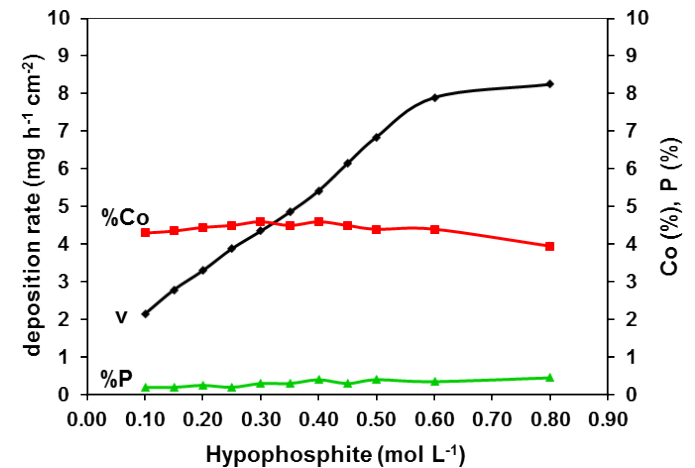


Fig. 6 - Influence of hypophosphite concentration on deposition rate and alloy composition, for standard bath composition.

4.6. Effect of citrate

The observation of Fig.7 shows that the deposition rate decreases for citrate concentrations higher than 0.05 M in spite of the cobalt and phosphorus content remain practically constant, respectively, 4.6 % and 0.3 %. This behavior is explained by a speciation effect of citrate on the positive metallic ions in solution, i.e., in reducing Σ_{Cu} and Σ_{Co} concentrations. Thus, in those situations the system is operating under cathodic diffusional control.

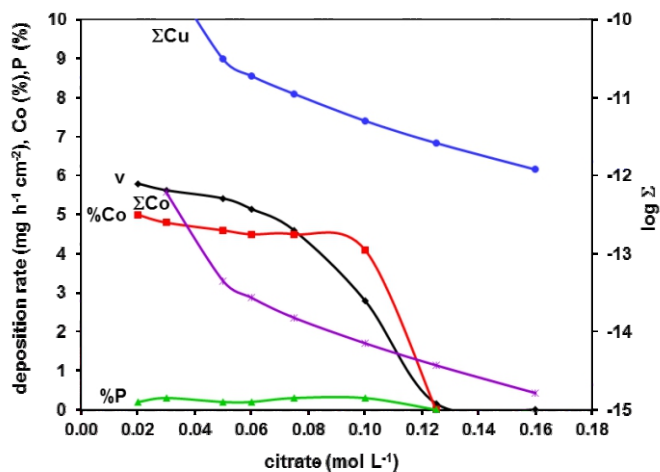


Fig. 7 - Influence of citrate concentration on deposition rate, ionic speciation of copper and cobalt positive ions, and alloy composition, for standard bath composition.

4.7. Effect of boric acid

The influence of boric acid on the deposition rate is synthesised in Fig. 8. The results allow saying that the buffering action is manifested in the ionic speciation of the bath. The deposition rate decreases with the concentration of boric acid due to decreasing concentrations of Σ_{Cu} and Σ_{Co} , which is consistent with the analysis made for the citrate. Eventually some specific action of the buffer on the substrate surface may also occur [10, 40].

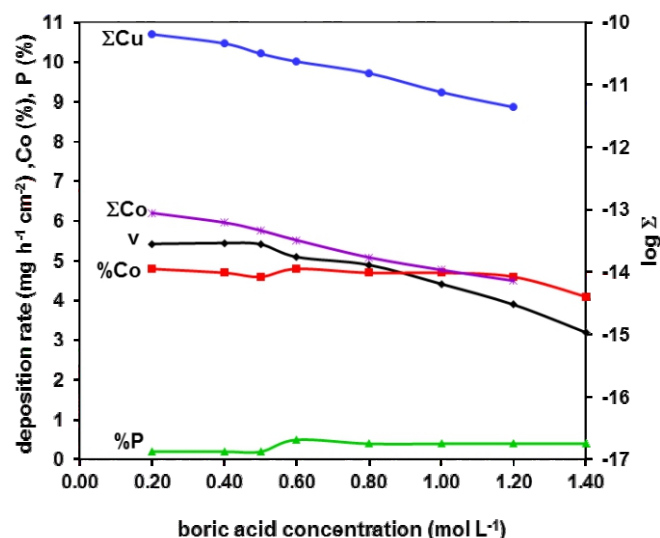
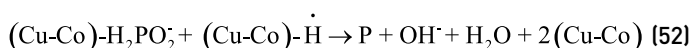


Fig. 8 - Influence of boric acid on deposition rate, ionic speciation of copper and cobalt positive ions, and alloy composition, for standard bath composition.

4.8. Effect of concentration ratio between $[CoSO_4]$ and $[CuSO_4] + [CoSO_4]$

Figure 9 shows that increasing the mole fraction of cobalt in the bath decreases the overall deposition rate. This negative effect is in agreement with the information contained therein: decrease of Σ_{Cu} , increase of Σ_{Co} , and increasing contents of Co and phosphorus in the coating.

Experimentally, it has been found that increased cobalt content in the bath promotes the release of hydrogen and the co-deposition of phosphorus according to the following reaction:



This reaction indicates that alkalinity reduces the content of phosphorus in the deposit in agreement with the results already discussed for pH.

The equilibrium phase diagrams of Co-P or Cu-P exhibit basically no solid solubility of phosphorus in cobalt or copper at ambient temperatures [33, 41]. The alloy is mainly pure copper, α -(Cu-Co) phase, and the possible intermetallic Co_2P and Cu_3P [42-44]. The increase of phosphorus content until 2% with the increase of MRC is responsible by appearing of a microcrystallinity.

Despite the decrease in Σ_{Cu} , but given that Σ_{Co} increases as well as the cobalt content in the deposit with MRC value, the decrease in deposition rate may be explained with the reduction in the active centers on surface due the presence of phosphorus atoms or the activation energy to promote the oxidation of hypophosphite on cobalt catalyst.

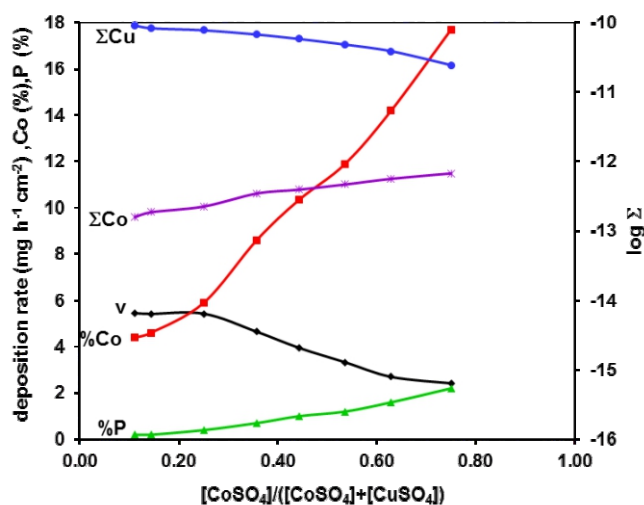


Fig. 9 - Influence of ratio between the catalyst and the amount of the catalyst plus metal, on deposition rate, ionic speciation of copper and cobalt positive ions, and alloy composition, for standard bath composition.

4.9. Effect of temperature

Table 3 shows the effect of temperature on the global deposition rate. The analyses of these results according to Arrhenius equation reveals activation energy of 51.4 kJ mol^{-1} . This system is under electrochemical control, i.e., the anodic reaction is controlled by activation energy of the hypophosphite on the copper-cobalt alloys, which matches with the analysis performed for the MRC effect.

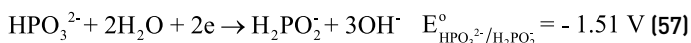
Table 3 - Effect of bath (standard composition with $[Co^{2+}] = 2 \times 10^{-3} \text{ M}$) temperature on the deposition rate, and on cobalt and phosphorus content in the films.

Temperature [°C] →	40	55	60	65	70	75	80	85
$v \text{ (mg cm}^{-2}\text{h}^{-1}\text{)}$	1.1	3.3	4.5	5.2	7.1	7.7	8.5	9.6
% Co	3.1	3.7	3.8	4.6	4.4	4.5	4.7	4.5
% P	0.5	0.3	0.4	0.3	0.3	0.5	0.4	0.5

4.10. Potential of electroless deposition

Monitoring the potential of aluminum substratum (Fig. 10), through the copper-cobalt alloy deposition from standard composition of the bath, proved the existence of three stages: 1) At first, the negative potential associated with the aluminum solubilization increases sharply to a maximum, which is associated with the deposition of copper and cobalt by chemical shift; 2)

Second, there is again a potential return to more negative values but less steeply than in the first stage to a minimum value, i.e., polarization phenomena, and at this stage the metal deposition derives from the oxidation of hypophosphite; 3) In the third step the potential remains constant, around -1.028 V vs SCE, and corresponds to the mixed potential. Li and Kohl [45] have observed that the steady OCP for copper deposition from a similar bath composition using nickel as catalyst is between -0.981 and -1.064 V vs SCE, and Martins *et al* [22] -0.997 V vs Ag/AgCl (1.0 M KCl). It should be noted that for the sample without catalyst in the bath, MRC = 0, takes place solely the first stage of deposition, i.e., no growth of the deposit. According to the electrochemistry, the standard reduction potential of copper, cobalt, phosphite and hypophosphite are shown as follows [46]:



To estimate the theoretical open circuit potential for the above reactions it has been considered that standard potential is a linear function of temperature.

$$E_T^{\circ} = E_{298}^{\circ} + (T-298.15) \left(\frac{dE^{\circ}}{dT} \right)_{298} \quad (58)$$

According to the results of the effect of time on plating rate for the standard bath composition we can say that the system is under steady-state, i.e., both bath and alloy composition are practically constant. Then, taking into account the ionic speciation of the standard bath composition ($[\text{Cu}^{2+}] = 5.6 \times 10^{-14}$ M; $[\text{Co}^{2+}] = 7.4 \times 10^{-15}$ M; $[\text{H}_2\text{PO}_2^{-}] = 0.27$ M; pH = 10) and supposing a concentration of phosphide ion around 10^{-20} M, it was obtained the following open circuit potentials for the above described reactions:

$$E_{\text{Cu}^{2+}/\text{Cu}}^* = -0.061 \text{ V}; \quad E_{\text{H}^{+}/\text{H}_2}^* = -0.590 \text{ V}; \quad E_{\text{Co}^{2+}/\text{Co}}^* = -0.708 \text{ V};$$

$$E_{\text{H}_2\text{PO}_2^{-}/\text{P}}^* = -1.486 \text{ V}; \quad E_{\text{HPO}_3^{2-}/\text{H}_2\text{PO}_2^{-}}^* = -1.729 \text{ V};$$

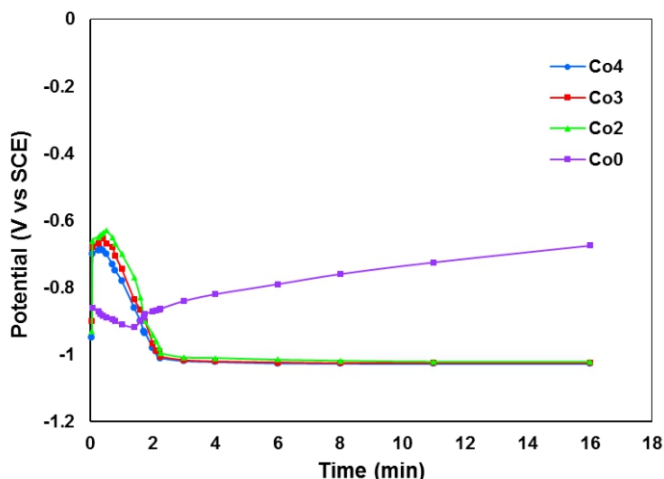


Fig. 10 – Evolution of potential along the electrodeposition of the copper-cobalt alloy: Co4, MRC = 0.75; Co3, MRC = 0.50; Co2, MRC = 0.238; Co0, MRC = 0.

Assuming the validity of the mixed potential theory for electroless copper deposition, it is sketched in Fig.11 the respective Evans diagram. Clearly, the deposition of phosphorus cannot be explained by the electrode reaction (56), since its open circuit potential is lower than the deposition potential at which the system operates. Thus, reaction (52) is more consistent, i.e., the formation of phosphorus from a radical reaction: the hydrogen radical in the active centers of the Cu-Co interacts with hypophosphite and promotes the alloying of P into Cu-Co.

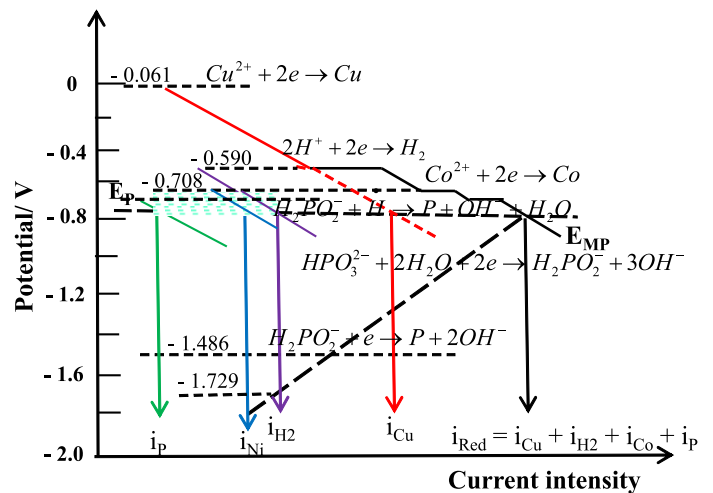


Fig. 11 – Sketch of Evans diagram for the electrode reactions in the electroless copper plating system according to the theory of mixed potential.

5. CONCLUSIONS

A chemical model based on reversible reactions has been established to determine ionic speciation into electroless copper plating baths. The values of Σ_{Cu} and Σ_{Co} , associated with the alloy composition and microstructure allow understanding the influence of the plating factors on the kinetics of copper deposition.

The effect of pH on the deposition rate shows that the cathodic reaction has to be extended to the cationic complexes of copper with the hydroxyl ions. Increasing the pH decreases slightly the cobalt and phosphorus contents.

The action of the hypophosphite shows for higher concentrations that the cathodic reaction is controlled by diffusion, and that the maximum deposition rate is $8.3 \text{ mg cm}^{-2} \text{ h}^{-1}$ for the following conditions: $0.024 \text{ M CuSO}_4 \cdot 5\text{H}_2\text{O}$, $0.60 \text{ M NaH}_2\text{PO}_2 \cdot \text{H}_2\text{O}$, $0.052 \text{ M Na}_2\text{C}_6\text{H}_5\text{O}_7 \cdot 2\text{H}_2\text{O}$, $0.50 \text{ M H}_3\text{BO}_3$, $0.004 \text{ M CoSO}_4 \cdot 6\text{H}_2\text{O}$, pH = 10.0 and temperature 65°C .

The calculated activation energy of 51.4 kJ mol^{-1} shows that the system is under electrochemical control. Increasing the $[\text{CoSO}_4] / ([\text{CoSO}_4] + [\text{CuSO}_4])$ ratio above 0.25, despite the increase of Σ_{Co} and cobalt content in the alloy, the deposition rate is successively lower. This is due to the increase of phosphorus content in the alloy that may poison the active centers and/or the change of activation energy of hypophosphite oxidation with the alloy composition. The morphology of the alloys is changed, of a uniform cubic crystalline structure to a globular structure, with the increase of MRC value of 0.111 to 0.750, but the structure remains crystalline in spite of phosphorus content 2%.

The operating potential of the system for the standard composition of the bath is -1.028 V vs SCE, but the open circuit potential for the deposition of phosphorus from phosphite, according to ionic speciation of the plating bath is -1.486 V vs NHE. This confirms the electrocatalytic oxidation of hypophosphite by dehydrogenation. Thus, the deposition of phosphorus in the Cu-Co-

P alloy can be explained by the interaction of an H atom removed from P-H bond with a new molecule of hypophosphite.

The use of cobalt ions instead of nickel ions allows obtaining copper-cobalt deposits with levels of phosphorus in the order of 0.2-0.3 %, and consequently doesn't change significantly the properties of these metallic coatings.

Acknowledgements

The work has financial support from the UID/AUR/04509/2013 Project by FCTMEC through national funds and, where applicable, the FEDER co-financing under the new PT2020 partnership agreement. This work is dedicated to the memory of Professor Luísa Maria Abrantes.

REFERENCES

- J. Cai, M. Lan, D. Zhang and W. Zhang, Electrical resistivity and dielectric properties of helical microorganism cells coated with silver by electroless plating, *Appl. Surf. Sci.*, 258, 8769-8774 (2012).
- J. F. Rohan, G. O'Riordan and J. Boardman, Selective electroless nickel deposition on copper as a final barrier/bonding layer material for microelectronics applications, *Appl. Surf. Sci.*, 185, 289-297 (2002).
- M. Bazzioui, J. I. Martins, E. A. Bazzioui, A. Albourini, R. Wang and P. D. Hong, A simple method for acrylonitrile butadiene styrene metallization, *Surf. Coat. Tech.*, 224, 71-76 (2013).
- M. Bazzioui, J. I. Martins, E. A. Bazzioui and A. Albourini, Environmentally friendly process for nickel electroplating of ABS, *Appl. Surf. Sci.*, 258, 7968-7975 (2012).
- Y. Shacham-Diamand and V. M. Dubin, Copper electroless deposition technology for ultra-large-scale-integration (ULSI) metallization, *Microelectron. Eng.*, 33, 47-58 (1997).
- B. Ui, J. Li, Q. Zhao, T. Liang and L. Wang, Effect of CuSO₄ content in the plating bath on the properties of composites from electroless plating of Ni-Cu-P on birch veneer, *BioResources*, 9, 2949-2959 (2014).
- B. Hu, R. Sun, G. Yu, L. Liu, Z. Xie, X. He and X. Zhang, Effect of bath pH and stabilizer on electroless nickel plating of magnesium alloys, *Surf. Coat. Tech.*, 228, 84-91 (2013).
- L. M. Abrantes and J. P. Correia, On the mechanism of electroless Ni-P plating, *J. Electrochem. Soc.*, 141, 2356-2360 (1994).
- J. E. A. M. Van Den Meerakker, On the mechanism of electroless plating. II. One mechanism for different reductants, *J. Appl. Electrochem.*, 11, 395-400 (1981).
- A. Hung and K. M. Chen, Mechanism of hypophosphite-reduced electroless copper plating, *J. Electrochem. Soc.*, 136, 72-75 (1989).
- J. Dumesic, J. A. Koutsky and T. W. Chapman, The rate of electroless copper deposition by formaldehyde reduction, *J. Electrochem. Soc.*, 121, 1405-1412. (1974).
- T. Anik, M. E. Touhami, K. Himm, S. Schireen, R. A. Belkhamima, M. Abouchane and M. Cissé, Influence of pH solution on electroless copper plating using sodium hypophosphite as reducing agent, *Int. J. Electrochem. Sci.*, 7, 2009 - 2018 (2012).
- R. Touir, H. Larhzi, M. Ebntouham, M. Cherkaoui and E. Chassaing, Electroless deposition of copper in acidic solutions using hypophosphite reducing agent, *J. Appl. Electrochem.*, 36, 69-75 (2006).
- D. Plana, A. I. Campbell, S. N. Patole, G. Shul and R. A. Dryfe, Kinetics of electroless deposition: the copper-dimethylamine borane system, *Langmuir*, 26, 10334-10340 (2010).
- Y. Liao, S. Zhang and R. Dryfe, Electroless copper plating using dimethylamine borane as reductant, *Particuology*, 10, 487-491 (2012).
- C. Xu, G. Liu, H. Chen, R. Zhou and Y. Liu, Fabrication of conductive copper-coated glass fibers through electroless plating process, *J. Mater. Sci.-Mater. El.*, 25, 2611-2617 (2014).
- L. You, L. Guo, R. Preisser and R. Alkolkar, Autocatalysis during Electroless Copper Deposition using Glyoxylic Acid as Reducing Agent, *J. Electrochem. Soc.*, 160, D3004-D3008 (2013).
- M. Selvam, Electroless silver deposition on ABS plastic using Co(II) as reducing agent, *Transactions of the IMF*, 88, 198-203 (2010).
- M. Sone, K. Kobayakawa, M. Saitou and Y. Sato, Electroless copper plating using Fe(II) as a reducing agent, *Electrochim. Acta*, 49, 233-238 (2004).
- C. Y. Hung, H. C. Yuan, L. F. Der Lai, R. M. Loan, C. K. Nan and Y. J. Taut, Electroless deposition of the copper sulfide coating on polyacrylonitrile with a chelating agent of triethanolamine and its EMI Shielding Effectiveness, *Thin Solid Films*, 517, 4984-4988 (2009).
- M. W. Liang, H. T. Yen and T. E. Hsieh, Investigation of electroless cobalt-phosphorous layer and its diffusion barrier properties of Pb-Sn solder, *J. Electron. Mater.*, 35, 1593-1599 (2006).
- J. I. Martins and M. C. Nunes, On the kinetics of copper electroless plating with hypophosphite reductant, *Surface Eng.*, 32, 363-371 (2016).
- F. A. Cotton, L. M. Daniels, C. A. Murillo and J. F. Quesada, Hexaaqua dipositive ions of the first transition series: new and accurate structures; expected and unexpected trends, *Inorg. Chem.*, 32, 4861-4867 (1993).
- P. E. M. Wijnands, J. S. Wood, J. Reedijk and W. J. A. Maaskant, Disordered Cu₆ Jahn-Teller centers in hexakis(1-methyltetrazole)copper(II)tetrafluoroborate: a temperature-dependent X-ray diffraction and EPR study, *Inorg. Chem.*, 35, 1214-1222 (1996).
- C. Wagner and W. Traud, The analysis of corrosion procedures through the interaction of electrochemical partial procedures and on the potential difference of mixed electrodes, *Z. Electrochim.*, 44, 391-402 (1938).
- A. J. Bard and L. R. Faulkner, *Electrochemical Methods: fundamental and applications*, John Wiley & Sons, Inc., Toronto (1980).
- J.-A. Dean, *Lange's: Handbook of Chemistry*, 11th ed., McGraw-Hill, New York (1973).
- E. Campi, G. Ostacoli, M. Meirone and G. Saini, Stability of the complexes of tricarballic and citric acids with bivalente ions in aqueous solution, *J. Inorg. Nucl. Chem.*, 26, 553-564 (1964).
- National Institute of Standards and Technology (NIST) thermochemical database 46 version 7, 2003.
- E. Högfeldt, *Stability constants of Metal-Ion Complexes: Part A. Inorganic ligands*, Pergamon, Oxford (1982).
- K. E. Atkinson, *An Introduction to Numerical Analysis*, John Wiley & Sons, Inc., (1989).
- JCPDS International Center for Diffraction Data, Swarthmore, 1997, Pennsylvania, U.S.A., copper file no. 04-0836.
- M. Hansen and K. Anderko, *Constitution of Binary Alloys*, McGraw-Hill, New York, 1958. Translated under the title *Struktury dvoynykh splavov*, Moscow: Metal-lurgiya, vol. 1, p. 624 (1962).
- V. V. Povetkin and O. V. Devyatkov, Codeposition of Copper and Cobalt from Trilonate Baths and the Properties of the Alloys Produced, *Prot. Met.*, 37, 314-316 (2001).
- Z. Chang, Y. Chang, J. Xu, Z. Wu, J. Xu, H. MA and Z. Lei, Structures and properties characterization of acrylonitrilebutadiene-styrene /organo-palygorskite clay composites, *Journal of Wuhan University of Technology-Mater. Sci. Ed.*, 27, 1068-1071 (2012).
- C.M.B. Martins and J. I. Martins, Mechanism of corrosion of roman coins from Senhora do Castelo, *Corros. Prot. Mater.*, 28, 126-133 (2009).
- I. Ohno, O. Wakabayashi and S. Haruyama, Anodic oxidation of reductant in electroless plating, *J. Electrochem. Soc.*, 132, 2323-2330 (1985).
- Y. Zeng, Y. Zheng, S. Yu, K. Chen and S. Zhou, An ESR study of the electrocatalytic oxidation of hypophosphite on a nickel electrode, *Electrochim. Commun.*, 4, 293-295 (2002).
- G. Gutzeit, An outline of the chemistry involved in the process of catalytic nickel deposition from aqueous solution. Part (IV), *Plating*, 47, 63-70 (1960).
- Y. Tsuru, M. Nomura, F. R. Foulkes, Effects of boric acid on hydrogen evolution and internal stress in films deposited from a nickel sulfamate bath, *J. Appl. Electrochem.*, 32, 629-634 (2002).
- D. T. Hawkins and R. Hultgren, *Metals Handbook*, 8th ed., Vol. 8, Lyman, Taylor, American Society for metals (1973).
- I. Kosta, A. Vicenzo, C. Müller and M. Sarret, Mixed amorphous-nanocrystalline cobalt phosphorous by pulse plating, *Surf. Coat. Techn.*, 207, 443-449 (2012).
- K. M. Nam, J. H. Shim, H. Ki, S. I. Choi, G. Lee, J. K. Jang, Y. Jo, M. H. Jung, H. Song and J. T. Park, Single-crystalline hollow face-centered-cubic cobalt nanoparticles from solid face-centered-cubic cobalt oxide nanoparticles, *Angew. Chem. Int. Ed.*, 47, 9504-9508 (2008).
- Hui-Sheng Yu, Shou-Fu Luo and Yong-Rui Wang, A comparative study on the crystallization behavior of electroless Ni-P and Ni-Cu-P deposits, *Surf. Coat. Techn.*, 148, 143-148 (2001).
- J. Li and P. A. Kohl, The deposition characteristics accelerated nonformaldehyde electroless copper plating, *J. Electrochem. Soc.*, 150, C558-C562. (2003).
- S. G. Bratsch, Standard electrode potentials and temperature coefficients in water at 298.15 K, *J. Phys. Chem. Ref. Data*, 18, 1-21 (1989).